Supplementary Materials for

Coupling organelle inheritance with mitosis to balance growth and differentiation

Amma Asare, John Levorse, Elaine Fuchs*

*Correspondence to: fuchslb@rockefeller.edu

Published 3 February 2017, *Science* **355**, eaah4701 (2017)
DOI: 10.1126/science.aah4701

This PDF file includes:

Other Supplementary Material for this manuscript includes the following:
(available at www.sciencemag.org/content/355/6324/eaah4701/suppl/DC1)

Materials and Methods

RNA-seq and Analysis

FACS isolated keratinocytes were sorted directly into TrizolLS (Invitrogen). 4-12 embryos were pooled per condition. RNA was purified using Direct-zol RNA MiniPrep kit (Zymo Research) per manufacturer's instructions. 2 pooled samples ETH sequenced for each condition. Quality of the RNA for sequencing was determined using Agilent 2100 Bioanalyzer, all samples had RNA integrity numbers (RIN) > 8. Library preparation using Illumina TrueSeq mRNA sample preparation kit was performed at the Weill Cornell Medical College Genomic Core facility, and RNAs were sequenced on Illumina HiSeq 2000 machines. Reads were aligned with Tophat using mouse genome build mm9 build. Transcript assembly and differential expression was performed using Cufflinks with Ensembl mRNAs to guide assembly. Analysis of RNA-seq data was done using the cummeRbund package in R *(55)*. Differentially regulated transcripts were analyzed with Gene Set Enrichment Analysis (GSEA) to find enriched gene sets *(56)*.

Flow Cytometry

Preparation of embryonic mouse back and head skin for isolation of keratinocytes was performed as previously described *(2)*. Briefly embryos and neonates: Skins were removed and treated with warm dispase for 1 hr at room temperature or overnight at 4ºC. The epidermis was peeled from the underlying dermis with forceps and placed into equal parts 0.25% Trypsin-EDTA and versene for 45 minutes at room temperature with shaking. E media was added to suspension to neutralize trypsin. Single-cell suspensions were obtained by filtering through a 70uM strainer and collected by centrifugation at 300g for 5 minutes. For detection of intracellular antigens including keratins, cells were washed in PBS and re-suspended at $1X10^6$ cells/0.1mL and 0.9mL 100% ice cold MeOH was slowly added while vortexing to fix cells. Cells were placed at -20ºC for >30 minutes. Cell suspensions were incubated with the appropriate antibodies for 30 minutes on ice. The following antibodies were used for FACS: α6-integrin (eBiosciences), CD140a (eBiosciences), CD31 (eBiosciences), CD45 (eBiosciences), K5 (Fuchs Lab), K10 (Covance), DAPI or LIVE/DEAD Fixable Aqua was used to exclude dead cells. Native keratin expression was used to isolate differentiating populations for RNAi screen. Transgenic keratins driving fluorescent histone expression was used to isolate intact cells for RNA extraction. Cell isolations were performed on FACS Aria sorters running FACS Diva software (BD Biosciences). For EdU incorporation experiments, staining was performed using Click-iT EdU Alexa Fluor 647 Flow Cytometry Kit (Life Technologies) per manufacturer's instructions. For cell cycle analysis MeOH fixed keratinocytes were stained with Dye Cycle Fx Violet (Invitrogen) per manufacturer instructions and cells were subsequently assayed. FACS analyses were performed using LSRII FACS Analyzers and results were analyzed with FlowJo vX software. Cells were prepared for ImageStream acquisition by fixation and staining just as they were prepared for FACS analysis.

Cell culture

1^0MKs from neonatal mouse skin were cultured in 0.05 mM Ca2+ or 1.5 mM Ca2+ media supplemented with 15% serum. For viral infections, keratinocytes were plated in 6-well dishes at 100,000 cells per well and incubated with lentivirus in the presence of polybrene (100 μg ml−1). After 2 days, we positively selected infected cells with

puromycin (1 μg/ ml−1) for 4–7 days, and processed them for mRNA and protein analyses. For 2X thymidine block cells were treated with 2mM thymidine (Sigma) for 19 hours released for 9 hours and treated again for > 12 hours.

Oxidase Activity Assay

2X10^6 Primary mouse keratinocytes knocked down for *shPex11b* or *shScr* were pelleted and flash frozen in liquid nitrogen. Cell pellets were re-suspended in PBS and assayed for oxidase activity as previously described *(57)*. Briefly, cell suspensions were mixed with H_20_2 and Triton X100. Air produced by the decomposition of H_20_2 creates foam which can be measured. Extracts from the peroxisome rich mouse liver were used as positive controls.

Time-lapse imaging

Keratinocytes were transduced with shRNAs, contained within a lentiviral vector harboring a puromycin resistance cassette. After ≥ 4 days, mRNA knockdown was confirmed by semi-quantitative RT-qPCR. Cells were then plated on glass-bottom dishes coated with fibronectin and acquired on a spinning-disc microscope equipped with a 40X air objective , 40X oil objective and an EM charge-coupled device camera (Hamamatsu). Additional plasmids used include GFP-PTS1 (Life Tech Cell light Peroxisome-GFP, BacMam 2.0 reagent #C10604), mCherry-tubulin and Krt14 H2B-GFP. Microtubules were imaged used SIR-Tubulin reagent at a concentration of 2.5nM. Cells were treated with SIR-Tubulin for 1 hour prior to imaging.

Optogenetic organelle transport

KIF1A-GFP-ePDZb1,PEX3-mRFP-LOV, BICD-ePDZb1 plasmids were a generous gift from C.Kapitein of Utrecht University (Netherlands). Plasmids were transiently co-transfected into keratinocytes using Effectene transfection reagent (Qiagen) and incubated with SIR-tubulin (Cytoskeleton) to mark microtubules. Light activation was performed as previously described *(51)*. Briefly, for wide field activation cells were exposed to blue spectrum light at intervals of 60 – 300s. Sequential imaging was taken of additional channels of interest. Early mitotic cells were found using early spindle formation as a marker then cells were exposed to blue light and a z-series was acquired at 2 minutes intervals for the next 1 -2 hours. For subsequent immunostaining 35mm plates were pulsed in temperature/CO_2 control chamber with blue light or kept in complete dark for 1 hour time course.

Barrier assay

Dye exclusion assays were performed as previously described *(58)*. Embryos are immersed in a low-pH X-gal substrate solution (100 μM NaPO4, 1.3 mM MgCl2, 3 mM K3Fe(CN)6, 3 mM K4Fe(CN)6, 1 mg ml−1 X-gal, 0.01% sodium deoxycholate, 0.2% NP-40, pH 4.5) at 30–37°C for several hours to overnight until color develops. Tails were snipped to serve as a positive control for staining. At low pH abundant β-galactosidase in the skin cleaves X-gal and forms a blue precipitate. This enzyme is only available to the substrate when the epidermis has incomplete barrier function.

Immunofluorescence and histological analyses

The following primary antibodies were used: chicken anti-GFP (1:2000; Abcam); guinea pig anti-K5 (1:500; E. Fuchs); rabbit anti-caspase 3 (AF835, 1:1000; R&D), guinea pig anti-RFP (1:1000, Fuchs), rabbit anti-K10 (PRB-159P, 1:1000; Covance), rabbit anti-filaggrin (PRB-417P, 1:2000; Covance), rabbit anti-Laminin 5 (1:1000, Fuchs), rabbit anti-PMP70 (1:500, Abcam), rabbit anti-Involucrin (1:2000, Covance),

rabbit anti-Hes1 (1:5000, Fuchs), mouse anti-γ tubulin (1:500, Sigma), rabbit anti-LGN (1:10000, Fuchs), rabbit anti-NuMA (1:500, Abcam), rabbit anti-pericentrin (1:500, Covance), and rabbit anti-survivin (1:500, Cell signaling). MitoTracker Orange CMTMRos (ThermoFisher Scientific #M7510), and 2.5nM SIR-tubulin (Cytoskeleton #Cy-SC006) reagents were used to label mitochondria and tubulin.

Frozen sections were cut at a thickness of 8–10 μm on a Leica cryostat and mounted on SuperFrost Plus slides (Fisher). Slides were air-dried for 30 min, then fixed for 10 min with 4% paraformaldehyde, rinsed with PBS, then blocked for 1 h in block (5% NDS, 1% BSA, 0.1% Triton X-100 in PBS) before incubating in primary antibody diluted in block at 4 °C overnight. After washing, secondary antibodies conjugated to Alexa-488, Alexa-647 (Molecular Probes), RRX, Alexa-546, or FITC were added for 1hr at room temperature. Slides were washed, counterstained with DAPI (0.5 μg ml−1) and mounted in ProLong Gold Antifade (Invitrogen). Imaging was performed on a Zeiss Axio Observer.Z1 epifluorescence microscope equipped with a Hamamatsu ORCA-ER camera (Hamamatsu Photonics), and with an ApoTome.2 (Carl Zeiss) slider that reduces the light scatter in the fluorescent samples controlled by Zen software (Carl Zeiss).

Back-skin thickness was quantified by taking >40 measurements per embryo of RFP+ regions from five random ×20 fields arrayed from anterior to posterior. Epidermal thickness was measured as the distance from the basement membrane (labelled with β4 integrin) to the skin surface. Peroxisome quantification was done using the ImageJ particle analysis plugin on 0.5μm Z-slices of epidermis immunostained for PMP70, a marker of peroxisomes, and phalloidin, a marker of cell boundaries.

Immunoblotting

Gel electrophoresis was performed using 4–12% NuPAGE Bis-Tris gradient gels (Invitrogen), transferred 1hr at 4ºC at 100 mA to nitrocellulose membranes. Membranes were blocked for 1 h in 5% milk-TBST, then incubated with primary antibodies in block overnight at 4 °C with gentle agitation. Membranes were rinsed several times in PBST (PBS + 0.1% Tween-20) before incubating in secondary antibodies diluted in block for 1hr at room temperature in the dark. Membranes were washed in PBST before developing blot. Quantification of band intensities was performed using ImageJ gel quantifier plug-in software. Primary antibodies used were: rabbit anti-pH3 (S10) (1:1000), mouse IgG anti-β-actin (Sigma, 1:5,000), rabbit anti-Hprt1 (Abcam, 1:2,000), rabbit anti-Pex11b (Sigma, 1:500), rabbit anti-Pex19 (Novus, 1:2000), rabbit-Acox1 (Sigma, 1:1000), rabbit anti-Catalase (Abcam, 1:1000).

RT–qPCR

mRNA was isolated using Direct-zol RNA MiniPrep kit (Zymo Research) per manufacturer's instructions and was quantified using a Nanodrop spectrophotometer. cDNA was synthesized from 250 ng of total RNA using Superscript III with oligo-dT primers (Invitrogen). cDNAs were mixed with indicated primers and SYBR green PCR Master Mix (Sigma), and qRT-PCR was performed on an Applied Biosystems 7900HT Fast Real-Time PCR system. Relative quantification was performed with data normalized to cyclophilin (Ppib) and Hprt1. To confirm the functionality of the primer sets used specificity was confirmed by the absence of product in samples prepared without reverse transcriptase (−RT controls); and product sizes calculated by melting curve analysis.

Mice, RNAi screen and lentiviral transduction

Mice were housed and cared for in an AAALAC-accredited facility, and all animal experiments were conducted in accordance with IACUC-approved protocols. CD1 mice were used for single gene knockdown experiments. The screen was performed in a C57/Bl6 background with 4 biological replicates of 6-10 pups each. shRNAs included in the screen and for all knock down experiments are from Sigma TRC 1.0 or 1.5 mouse library. Based on a library targeting ~810 genes each screen replicate had a coverage of >75X.

We used non-invasive, ultrasound-guided in utero lentiviral-mediated delivery of RNAi, which selectively transduces single-layered surface ectoderm of living E9.5 mouse embryos as previously described (*54*). All shRNAs were obtained from The Broad Institute's Mission TRC-1 mouse library, and were present in the pLKO.1 lentiviral backbone, which harbors a puromycin-resistance cassette. shRNA sequences were cloned from the library vectors into our modified pLKO H2B-mRFP1, H2B-YFP, or H2B-CFP vectors and high titer lentivirus was produced as previously described(*54*).

Deep Sequencing: Sample preparation, pre-amplification and sequence processing

Keratinocytes isolated from FACS sorted P4 epidermis were subjected to genomic DNA isolation with the DNeasy Blood & Tissue Kit (Qiagen), and each sample was analyzed for target transduction using real-time PCR. 6μg genomic DNA of each cell population was used as template in a preamplification reaction with 21 cycles and Phusion High-Fidelity DNA Polymerase (NEB). PCR products were run on a 2% agarose gel, and a clean ~200 bp band was isolated using QIAquick Gel Extraction Kit as recommended by the manufacturer (Qiagen). Final samples were then sent for Illumina HiSeq 2000 sequencing. Illumina reads were trimmed to the 21 nt hairpin sequence using the FASTX-Toolkit and aligned to the TRC 2.x library with BWA (v 0.6.2)44 using a maximum edit distance of 3. Hits were ranked based on (a) numbers of shRNAs that targeted the gene and scored positively in the screen and (b) magnitude of alteration relative to shScr (c) absence of shRNAs targeting the same gene showing opposing effects relative to shScr.

Statistical Analyses

Data were analyzed and statistics performed (unpaired or paired two-tailed student's t-tests or chi-squared tests). For determination of angles during mitosis, the number of cells analyzed (n) is indicated in the figure legends, and included cells from three or more embryos of the same age. Panels showing *shPex11b* include average values for 2-3 shRNAs targeting *Pex11b.* Error bars represent SEM in all plots. Boxplots show 25^{th} and 7^{5th} percentiles as top and bottom of box and center line as the median. Density plots show unit-less kernel density estimates of populations similar to smoothed histograms. All graphs were prepared in R graphical environment using ggplot2.

Fig. S1.

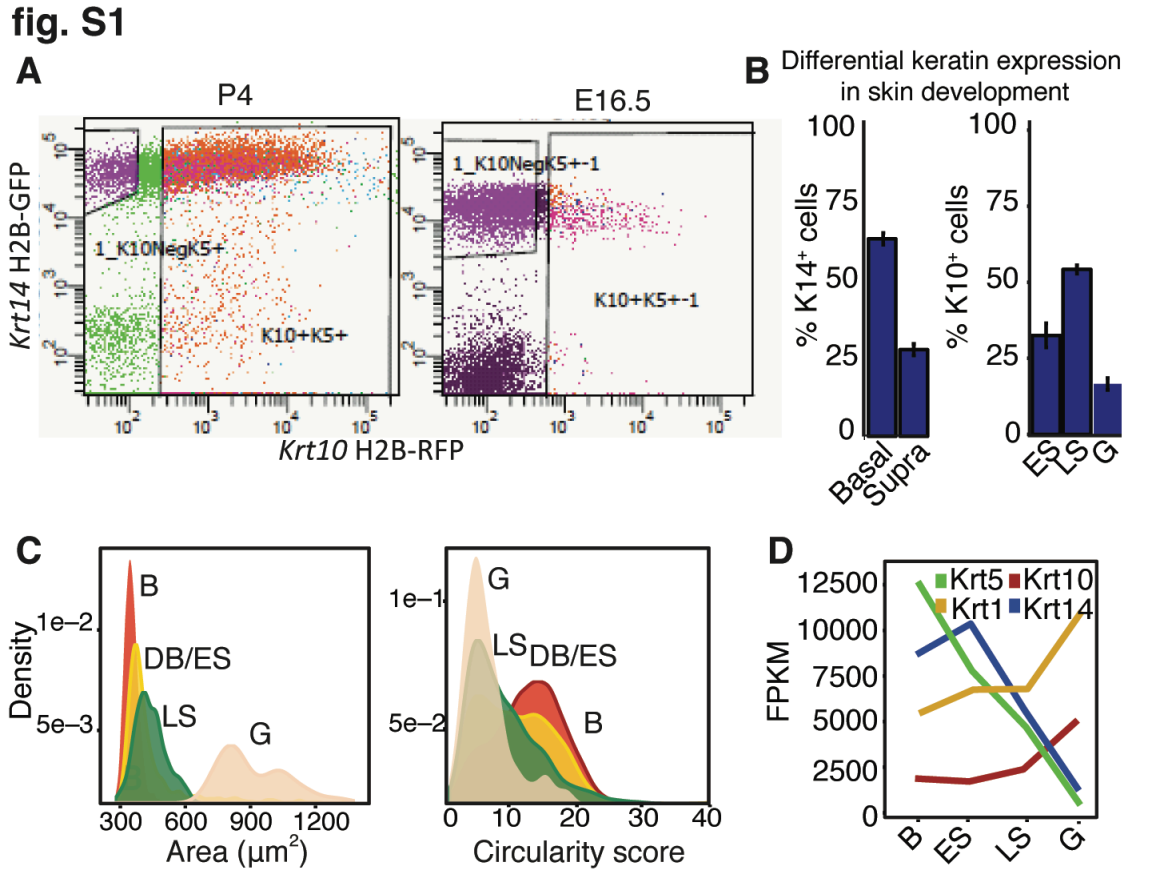

Use of Krt14 and Krt10 reporter mice in FACS separation of epidermal progenitors and progeny. A, Flow plots of epidermal keratinocytes from E16.5 and P4 skin transgenic for Krt14-H2B-GFP and Krt10-H2B-RFP. B, Quantification of flow cytometry analysis of keratin expression in P4 epidermis. Epidermis can be sub-divided into basal (K5+) and suprabasal (K5+K10+) cells. Keratin 10+ suprabasal cells can be further sub-divided into spinous and granular layers by expression of α6 integrin and cell size/granularity as shown in Main Fig. 1. C, Dramatic changes in cell size and shape upon epidermal differentiation. Quantifications of size and shape changes in epidermal layers from Image Stream analysis of P4 differentiating populations. Basal (B), Early spinous/ Differentiating Basal (DB/ES), Late spinous (LS), and Granular (G). D, FPKMs (fragment per kilobase million) of keratin transcripts from RNA sequencing of P4 epidermis for basal (B), early spinous (ES), late spinous (LS), and granular (G) cell populations. Keratins 5 and 14, markers of relatively undifferentiated keratinocytes are highly expressed in basal and early spinous layer while keratins 10 and 1 increase in differentiated layers.

Fig. S2

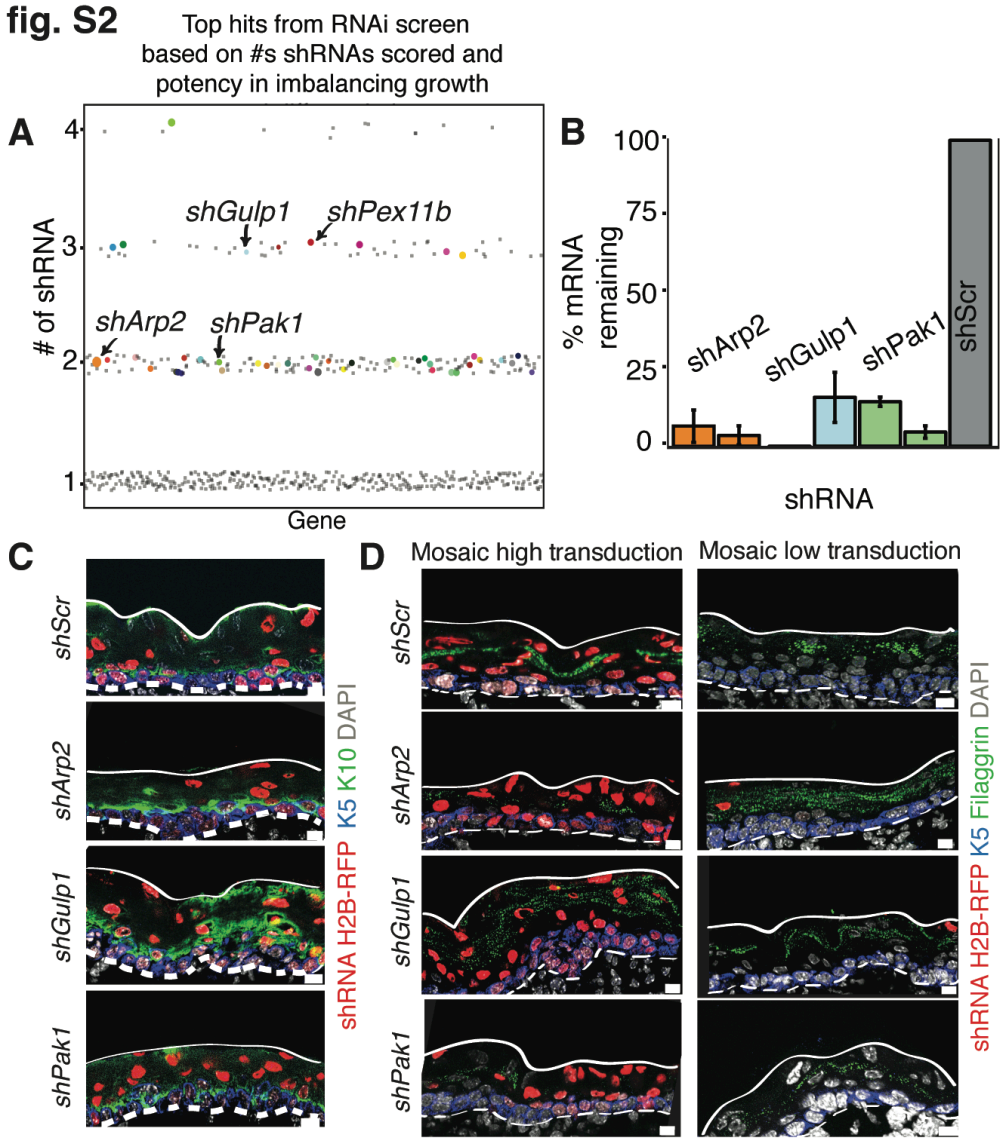

In vivo RNAi screen data and analyses. A, Dot plot of each gene in the screen as a single dot along x-axis and the number of shRNAs/gene showing a >2 Log2 change along y-axis. Location of validation genes is indicated by arrows. Results shown for a single screen replicate. Size of dot corresponds to the magnitude of the change in clone size. B, Semi-quantitative RT-qPCR quantification of knockdown efficiency of validation shRNAs in vitro. All genes show > 75% reduction in target mRNA expression. C,D, E16.5 sagittal sections of epidermis transduced with shRNAs targeting screen validation genes and probed for expression of keratin proteins and differentiation marker, filaggrin. After clonal transduction regions of high and low transduction within mosaic skin were analyzed. E, Scale bars = 10μm. Dashed white line marks basement membrane and solid white line marks skin surface.

Fig. S3

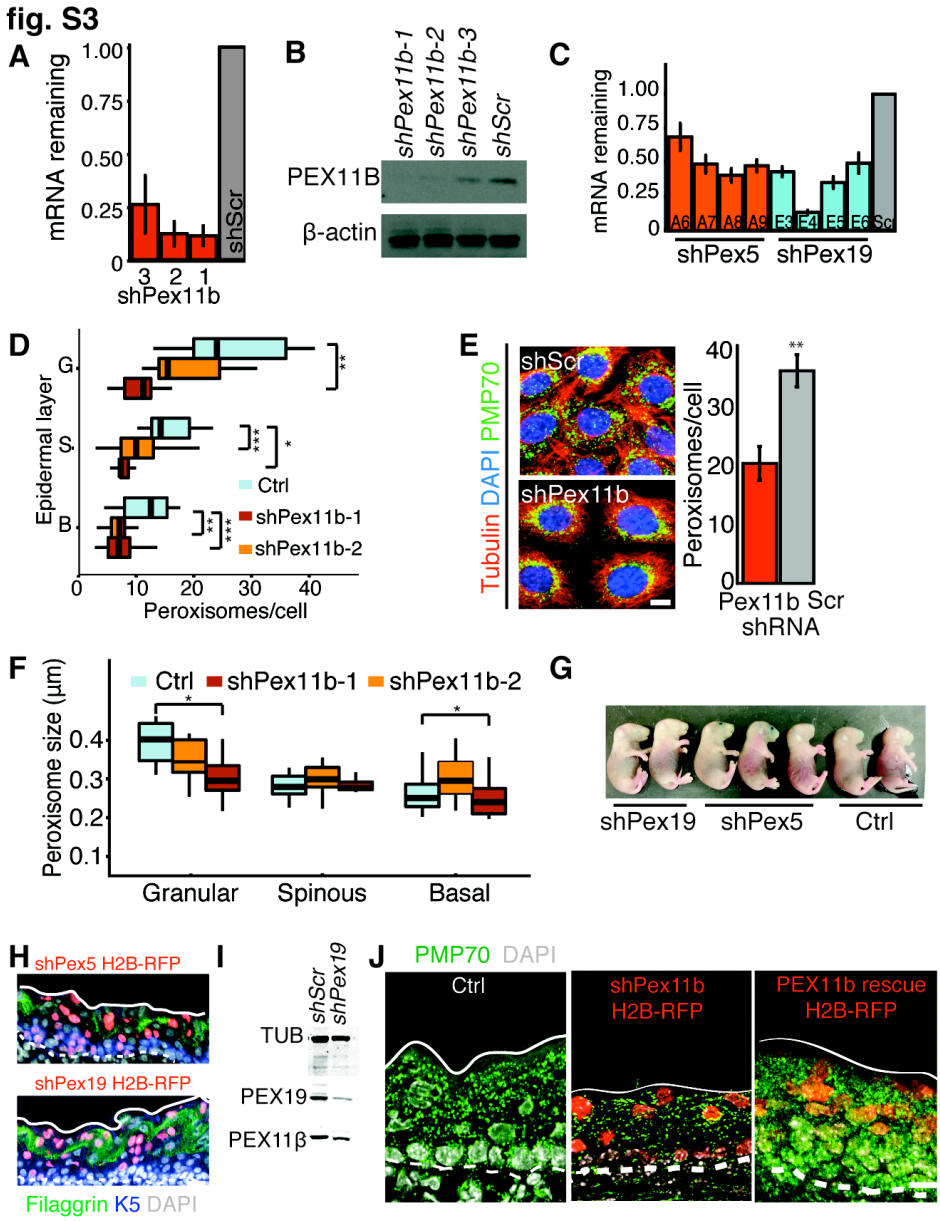

shPex11b, shPex19 and shPex5 analyses. A, Semi-quantitative RT-qPCR quantification of knockdown efficiency of validation shRNAs in vitro. All genes show > 75% reduction in target mRNA expression. B, Immunoblot for PEX11b 4 days after knockdown in vitro with shRNAs shPex11b-1, shPex11b-2, shPex11b-3. C, Semi-quantitative RT-qPCR quantification of knockdown efficiency of validation shRNAs in vitro. D,E,F, Quantification of peroxisome number and size from E16.5 epidermis or keratinocytes. Numbers of peroxisomes marked with PMP70 per cell per 0.5uM z-section were counted. G, Representative images from embryos after outside-in barrier assay. If the skin barrier

is incomplete, embryos will absorb blue dye. While this happens for shPex11b (see Main Fig. 3), it does not for shPex5 or shPex19. n=8 shPex19, n=6 shPex5, n=12 control littermates. H, Images from immuno-labeled E16.5 epidermis depleted for Pex5 or Pex19 and probed for granular differentiation marker filaggrin. Note proper expression patterns and normal epidermal thickness in skin of embryos depleted for these peroxins. I, Immunoblot for PEX19 and PEX11b in shPex19 keratinocytes showing appreciable retention of PEX11b protein despite marked reduction in peroxisomes resulting from PEX19 loss. J, Images from immuno-labeling for peroxisome marker PMP70 in skin sections of E16.5 embryos transduced with shPex11b ± a hairpin-resistant Pex11b cDNA expression vector.

Fig. S4

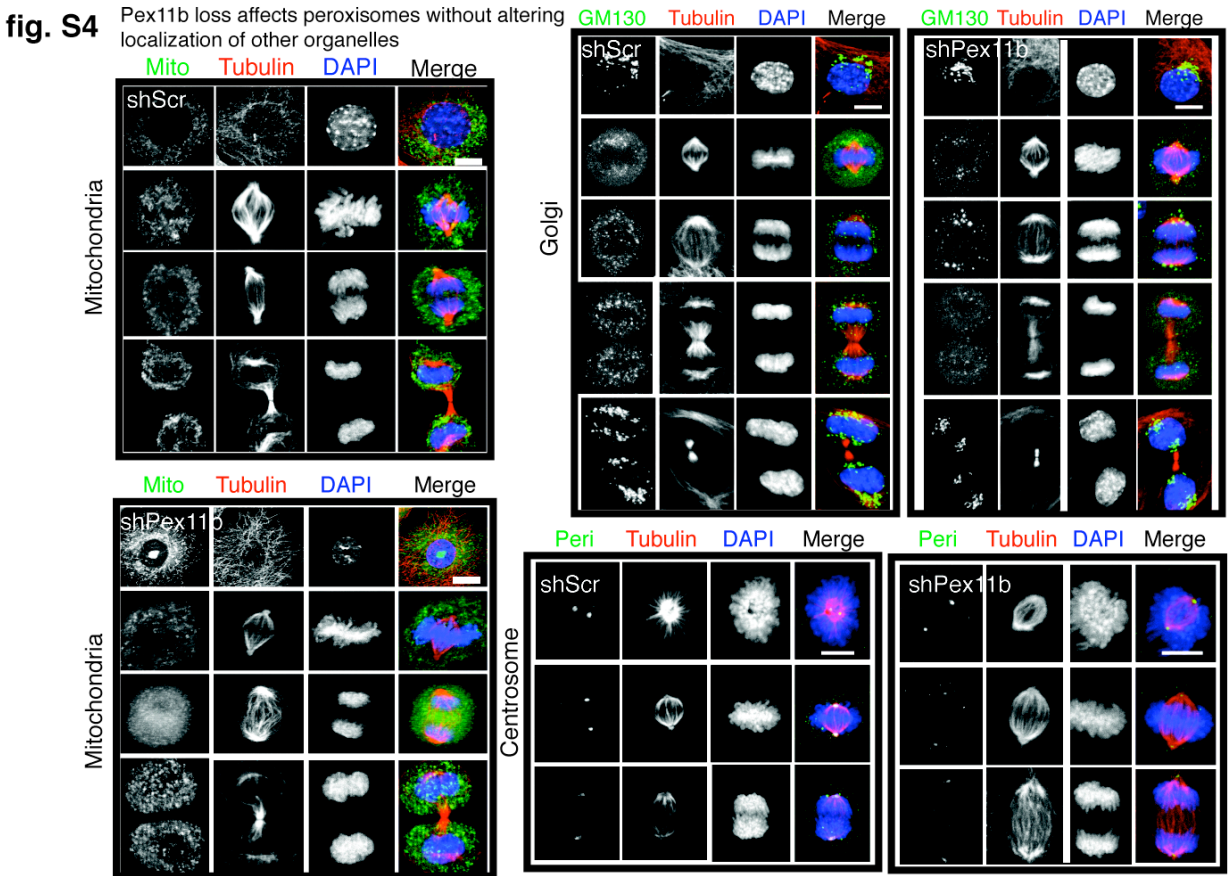

Proper localization and partitioning of golgi, centrosomes and mitochondria in *shPex11b* epidermal cells. 1^0MKs probed for golgi marker GM130 and for pericentrin or treated with MitoTracker to mark mitochondria. Representative images of cells in interphase, metaphase, anaphase and telophase are shown. Note similar localization of these other organelles through mitosis for *shScr* and *shPex11b*. n=30-50 mitotic cells per organelle type.

Fig. S5

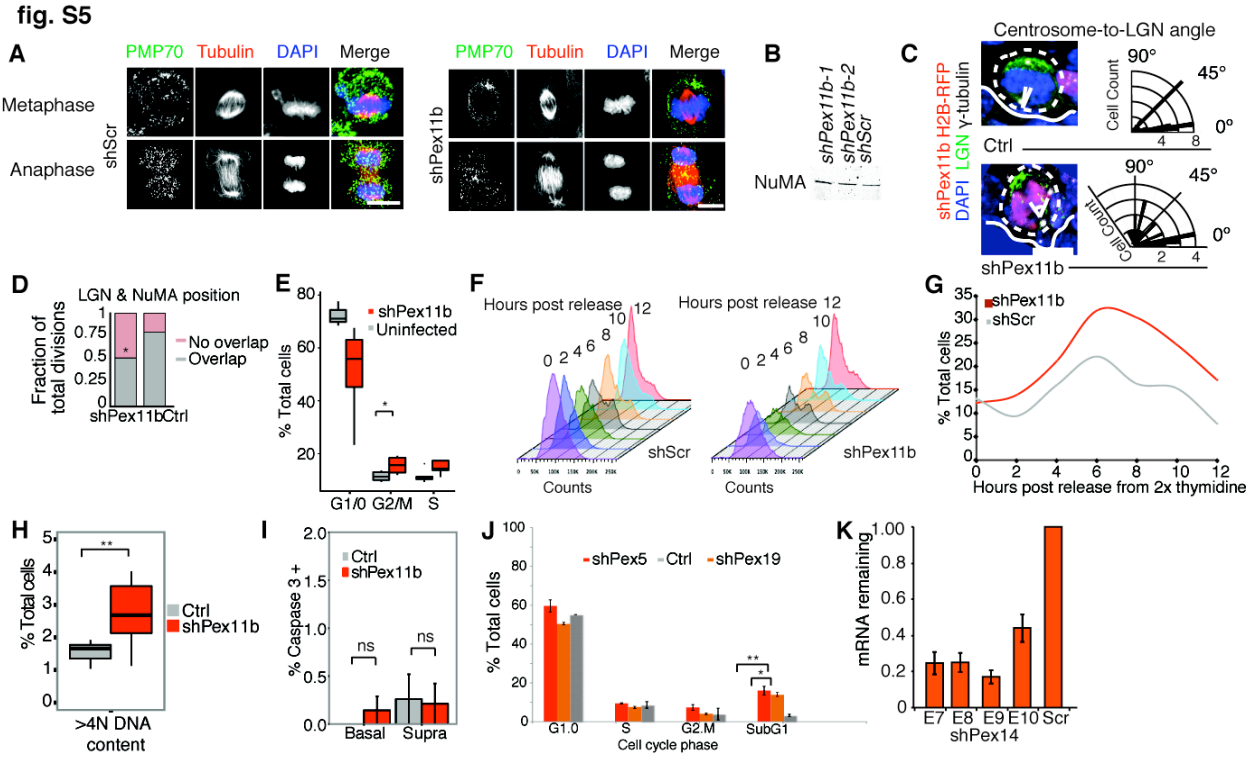

Mitotic alterations induced by PEX11b deficiency. A, Peroxisome localizations in metaphase and anaphase cells. Note that peroxisomes take on unusual cortical positions in metaphase when PEX11b is lost. Representative mitotic cells probed for PMP70 (peroxisome marker), tubulin and DAPI are shown. B, Immunoblots for NuMA and tubulin (control) reveal equivalent NuMA levels in shScr and shPex11b keratinocytes. C, shPex11b-induced perturbations in spindle alignment in embryonic skin epidermis. Shown are representative images of mitotic basal progenitors (outlined by white dotted lines) from E17.5 sagittal sections. Immuno-labeling is for LGN, which is typically cortical and apical in asymmetrically dividing basal progenitors, and γ-tubulin, which marks the spindle poles that are typically perpendicular to the LGN crescent, through the ability of NuMA to bind to LGN and also astral microtubules. Note that LGN in the shPex11b cell is misaligned relative to the spindle axis, consistent with the failure of NuMA to associate with the cortical LGN crescent in shPex11b epidermal progenitors (see Main Fig. 5). Radial histogram quantifies LGN position relative to spindle axis from sagittal sections. Ctrl n = 46, shPex11b n= 38. Student's t-test of significance p-value = <0.001. D, Quantification of relative positions of LGN and NuMA in mitotic cells in E.17.5 clonally transduced shPex11b epidermis. n=50 shPex11b, n=64 Ctrl. Chi-square test of significance, p-value < .05. E, DNA content analysis for cell cycle profiling of E16.5 ex vivo epidermal cells showing an enrichment in G2/M cells in shPex11b clones. F and G, shScr and shPex11b keratinocytes were treated with 2X thymidine and released. Samples were collected every 2 hours for cell cycle analysis by flow cytometry. Cell cycle profiles (a) and quantifications (b) for 2 shPex11b shRNAs and 2 shScr is shown. Note increased cells retained in G2/M phase from 2 hrs post release. H, Flow cytometry

analyses of DNA reveals an increase in the number of cells with >4N DNA content when Pex11b is knocked down, indicative of mitotic abnormalities. I, Quantification of apoptotic caspase 3 + cells from sagittal sections of E16.5 shScr and shPex11b epidermis. No significant differences observed. J, DNA content analysis for cell cycle profiling of E16.5 ex vivo epidermal cells from shPex5 (n=7, 2 litters) and shPex19 (n=9, 3 litters) transduced embryos. Note the enrichment of apoptotic/sub G1 cells. PEX5 and PEX19 depletion display enhanced apoptosis but without alterations in S or G2/M populations. K, Semi-quantitative RT-qPCR for knockdown efficiency of four different Pex14 shRNAs in vitro.

Fig. S6

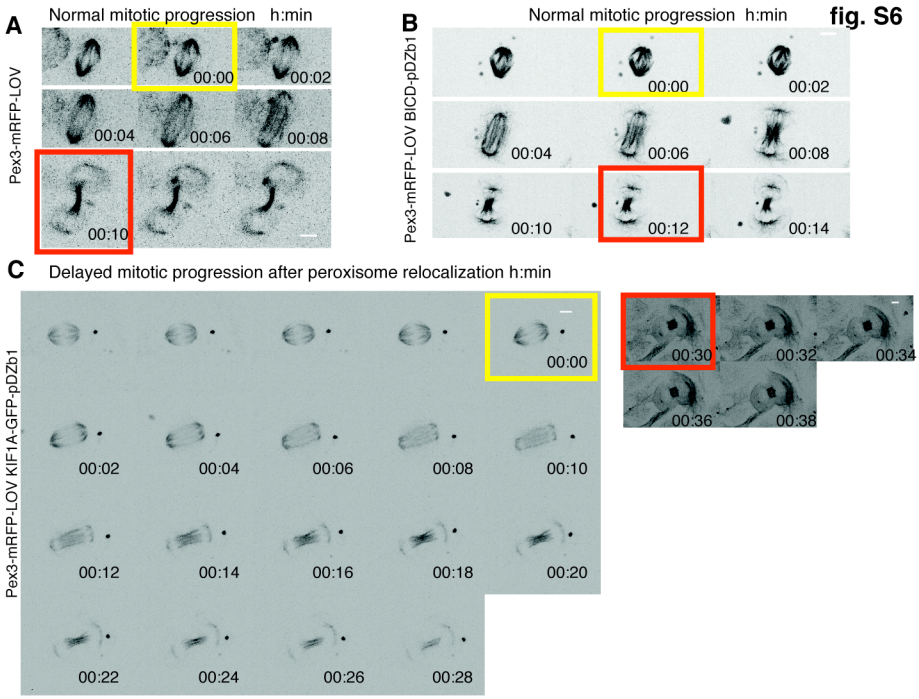

Mis-localization of peroxisomes is sufficient to trigger a mitotic delay. Epidermal keratinocytes were transfected with Pex3-mRFP-LOV (A) and either minus-end microtubule fusion protein, BICD-GFP-ePDZ1b (B) or plus-end microtubule motor fusion protein, KIF1A-GFP-ePDZ1b (C). Cells were time-lapse imaged over 1 hour after exposure to blue spectrum light. Shown are still frames from these movies. Yellow boxes show anaphase entry and red boxes highlight cytokinesis completion. Note increased anaphase time upon photo-activation of Pex3-mRFP-LOV keratinocytes doubly transfected with the plus-end motor construct, which brings peroxisomes to the spindle mid-zone, but not with the minus-end motor construct, which enhances both the duration and the concentration of peroxisomes at the spindle poles of mitotic cells.

Movie S1
shScr mitosis. shScr Primary cultured keratinocyte transfected with mCherry-Tubulin and pKrt14-H2B-GFP imaged in time-lapse at 3 minute intervals.

Movie S2
shPex11b mitosis. Primary cultured keratinocyte depleted of PEX11b and transfected with mCherry-Tubulin and pKrt14-H2B-GFP imaged in time-lapse at 3 minute intervals.

Additiional Data table S1 (separate file)
Individual shRNA performance in RNAi screen

Additiional Data table S2 (separate file)
Genes with ≥ two shRNAs more abundant in basal relative to suprabasal epidermal cells in the RNAi screen.

References

1. E. Fuchs, Finding one's niche in the skin. *Cell Stem Cell* **4**, 499–502 (2009). doi: 10.1016/j.stem.2009.05.001; Medline

2. S. E. Williams, S. Beronja, H. A. Pasolli, E. Fuchs, Asymmetric cell divisions promote Notch-dependent epidermal differentiation. *Nature* **470**, 353–358 (2011). doi: 10.1038/nature09793; Medline

3. T. Lechler, E. Fuchs, Asymmetric cell divisions promote stratification and differentiation of mammalian skin. *Nature* **437**, 275–280 (2005). doi: 10.1038/nature03922; Medline

4. S. J. Habib, B.-C. Chen, F.-C. Tsai, K. Anastassiadis, T. Meyer, E. Betzig, R. Nusse, A localized Wnt signal orients asymmetric stem cell division in vitro. *Science* **339**, 1445–1448 (2013). doi: 10.1126/science.1231077; Medline

5. C. Blanpain, W. E. Lowry, H. A. Pasolli, E. Fuchs, Canonical notch signaling functions as a commitment switch in the epidermal lineage. *Genes Dev.* **20**, 3022–3035 (2006). doi: 10.1101/gad.1477606; Medline

6. M. T. Niessen, J. Scott, J. G. Zielinski, S. Vorhagen, P. A. Sotiropoulou, C. Blanpain, M. Leitges, C. M. Niessen, aPKCλ controls epidermal homeostasis and stem cell fate through regulation of division orientation. *J. Cell Biol.* **202**, 887–900 (2013). doi: 10.1083/jcb.201307001; Medline

7. E. Clayton, D. P. Doupé, A. M. Klein, D. J. Winton, B. D. Simons, P. H. Jones, A single type of progenitor cell maintains normal epidermis. *Nature* **446**, 185–189 (2007). doi: 10.1038/nature05574; Medline

8. S. Beronja, P. Janki, E. Heller, W.-H. Lien, B. E. Keyes, N. Oshimori, E. Fuchs, RNAi screens in mice identify physiological regulators of oncogenic growth. *Nature* **501,** 185–190 (2013). doi: 10.1038/nature12464; Medline

9. E. Ezhkova, H. A. Pasolli, J. S. Parker, N. Stokes, I.-h. Su, G. Hannon, A. Tarakhovsky, E. Fuchs, Ezh2 orchestrates gene expression for the stepwise differentiation of tissue-specific stem cells. *Cell* **136,** 1122–1135 (2009). doi: 10.1016/j.cell.2008.12.043; Medline

10. A. Gandarillas, F. M. Watt, c-Myc promotes differentiation of human epidermal stem cells. *Genes Dev.* **11,** 2869–2882 (1997). doi: 10.1101/gad.11.21.2869; Medline

11. X. Li, S. J. Gould, PEX11 promotes peroxisome division independently of peroxisome metabolism. *J. Cell Biol.* **156,** 643–651 (2002). doi: 10.1083/jcb.200112028; Medline

12. I. Abe, K. Okumoto, S. Tamura, Y. Fujiki, Clofibrate-inducible, 28-kDa peroxisomal integral membrane protein is encoded by *PEX11*. *FEBS Lett.* **431,** 468–472 (1998). doi: 10.1016/S0014-5793(98)00815-1; Medline

13. J. Koch, K. Pranjic, A. Huber, A. Ellinger, A. Hartig, F. Kragler, C. Brocard, PEX11 family members are membrane elongation factors that coordinate peroxisome proliferation and maintenance. *J. Cell Sci.* **123**, 3389–3400 (2010). doi: 10.1242/jcs.064907; Medline

14. S. Kobayashi, A. Tanaka, Y. Fujiki, Fis1, DLP1, and Pex11p coordinately regulate peroxisome morphogenesis. *Exp. Cell Res.* **313,** 1675–1686 (2007). doi: 10.1016/j.yexcr.2007.02.028; Medline

15. M. A. Fox, L. A. Walsh, M. Nieuwesteeg, S. Damjanovski, PEX11β induces peroxisomal gene expression and alters peroxisome number during early *Xenopus laevis* development. *BMC Dev. Biol.* **11**, 24 (2011). doi: 10.1186/1471-213X-11-24; Medline

16. M. Schrader, B. E. Reuber, J. C. Morrell, G. Jimenez-Sanchez, C. Obie, T. A. Stroh, D. Valle, T. A. Schroer, S. J. Gould, Expression of *PEX11*β mediates peroxisome proliferation in the absence of extracellular stimuli. *J. Biol. Chem.* **273**, 29607–29614 (1998). doi: 10.1074/jbc.273.45.29607; Medline

17. H. K. Delille, B. Agricola, S. C. Guimaraes, H. Borta, G. H. Lüers, M. Fransen, M. Schrader, Pex11pβ-mediated growth and division of mammalian peroxisomes follows a maturation pathway. *J. Cell Sci.* **123,** 2750–2762 (2010). doi: 10.1242/jcs.062109; Medline

18. T. Orth, S. Reumann, X. Zhang, J. Fan, D. Wenzel, S. Quan, J. Hu, The PEROXIN11 protein family controls peroxisome proliferation in *Arabidopsis*. *Plant Cell* **19,** 333–350 (2007). doi: 10.1105/tpc.106.045831; Medline

19. P. A. Marshall, Y. I. Krimkevich, R. H. Lark, J. M. Dyer, M. Veenhuis, J. M. Goodman, Pmp27 promotes peroxisomal proliferation. *J. Cell Biol.* **129**, 345–355 (1995). doi: 10.1083/jcb.129.2.345; Medline

20. Y. Sakai, P. A. Marshall, A. Saiganji, K. Takabe, H. Saiki, N. Kato, J. M. Goodman, The *Candida boidinii* peroxisomal membrane protein Pmp30 has a role in peroxisomal proliferation and is functionally

homologous to Pmp27 from *Saccharomyces cerevisiae*. *J. Bacteriol.* **177,** 6773–6781 (1995). doi: 10.1128/jb.177.23.6773-6781.1995; Medline

21. P. B. Lazarow, Y. Fujiki, Biogenesis of peroxisomes. *Annu. Rev. Cell Biol.* **1,** 489–530 (1985). doi: 10.1146/annurev.cb.01.110185.002421; Medline

22. B. Ahlemeyer, M. Gottwald, E. Baumgart-Vogt, Deletion of a single allele of the *Pex11*β gene is sufficient to cause oxidative stress, delayed differentiation and neuronal death in mouse brain. *Dis. Model. Mech.* **5**, 125–140 (2012). doi: 10.1242/dmm.007708; Medline

23. X. Li, E. Baumgart, J. C. Morrell, G. Jimenez-Sanchez, D. Valle, S. J. Gould, PEX11β deficiency is lethal and impairs neuronal migration but does not abrogate peroxisome function. *Mol. Cell. Biol.* **22,** 4358–4365 (2002). doi: 10.1128/MCB.22.12.4358-4365.2002; Medline

24. M. S. Ebberink, J. Koster, G. Visser, F. van Spronsen, I. Stolte-Dijkstra, G. P. A. Smit, J. M. Fock, S. Kemp, R. J. A. Wanders, H. R. Waterham, A novel defect of peroxisome division due to a homozygous non-sense mutation in the *PEX11*β gene. *J. Med. Genet.* **49,** 307–313 (2012). doi: 10.1136/jmedgenet-2012-100778; Medline

25. A. M. Krikken, M. Veenhuis, I. J. van der Klei, *Hansenula polymorpha pex11* cells are affected in peroxisome retention. *FEBS J.* **276,** 1429–1439 (2009). doi: 10.1111/j.1742-4658.2009.06883.x; Medline

26. S. Huyghe, M. Casteels, A. Janssen, L. Meulders, G. P. Mannaerts, P. E. Declercq, P. P. Van Veldhoven, M. Baes, Prenatal and postnatal development of peroxisomal lipid-metabolizing pathways in the mouse. *Biochem. J.* **353**, 673–680 (2001). doi: 10.1042/bj3530673; Medline

27. A. Janssen, M. Baes, P. Gressens, G. P. Mannaerts, P. Declercq, P. P. Van Veldhoven, Docosahexaenoic acid deficit is not a major pathogenic factor in peroxisome-deficient mice. *Lab. Invest.* **80**, 31–35 (2000). doi: 10.1038/labinvest.3780005; Medline

28. J. M. Jones, J. C. Morrell, S. J. Gould, PEX19 is a predominantly cytosolic chaperone and import receptor for class 1 peroxisomal membrane proteins. *J. Cell Biol.* **164**, 57–67 (2004). doi: 10.1083/jcb.200304111; Medline

29. K. Götte, W. Girzalsky, M. Linkert, E. Baumgart, S. Kammerer, W.-H. Kunau, R. Erdmann, Pex19p, a farnesylated protein essential for peroxisome biogenesis. *Mol. Cell. Biol.* **18**, 616–628 (1998). doi: 10.1128/MCB.18.1.616; Medline

30. Y. Matsuzono, N. Kinoshita, S. Tamura, N. Shimozawa, M. Hamasaki, K. Ghaedi, R. J. A. Wanders, Y. Suzuki, N. Kondo, Y. Fujiki, Human *PEX19*: cDNA cloning by functional complementation, mutation analysis in a patient with Zellweger syndrome, and potential role in peroxisomal membrane assembly. *Proc. Natl. Acad. Sci. U.S.A.* **96**, 2116–2121 (1999). doi: 10.1073/pnas.96.5.2116; Medline

31. K. A. Sacksteder, J. M. Jones, S. T. South, X. Li, Y. Liu, S. J. Gould, PEX19 binds multiple peroxisomal membrane proteins, is predominantly cytoplasmic, and is required for peroxisome membrane synthesis. *J. Cell Biol.* **148**, 931–944 (2000). doi: 10.1083/jcb.148.5.931; Medline

32. J. Mathur, N. Mathur, M. Hülskamp, Simultaneous visualization of peroxisomes and cytoskeletal elements reveals actin and not microtubule-based peroxisome motility in plants. *Plant Physiol.* **128**, 1031–1045 (2002). doi: 10.1104/pp.011018; Medline

33. M. Schrader, S. J. King, T. A. Stroh, T. A. Schroer, Real time imaging reveals a peroxisomal reticulum in living cells. *J. Cell Sci.* **113** (Pt. 20), 3663–3671 (2000). Medline

34. L. Schollenberger, T. Gronemeyer, C. M. Huber, D. Lay, S. Wiese, H. E. Meyer, B. Warscheid, R. Saffrich, J. Peränen, K. Gorgas, W. W. Just, RhoA regulates peroxisome association to microtubules and the actin cytoskeleton. *PLOS ONE* **5**, e13886 (2010). doi: 10.1371/journal.pone.0013886; Medline

35. E. A. C. Wiemer, T. Wenzel, T. J. Deerinck, M. H. Ellisman, S. Subramani, Visualization of the peroxisomal compartment in living mammalian cells: Dynamic behavior and association with microtubules. *J. Cell Biol.* **136**, 71–80 (1997). doi: 10.1083/jcb.136.1.71; Medline

36. D. A. Collings, J. D. I. Harper, K. C. Vaughn, The association of peroxisomes with the developing cell plate in dividing onion root cells depends on actin microfilaments and myosin. *Planta* **218**, 204–216 (2003). doi: 10.1007/s00425-003-1096-2; Medline

37. C. Sütterlin, P. Hsu, A. Mallabiabarrena, V. Malhotra, Fragmentation and dispersal of the pericentriolar Golgi complex is required for entry into mitosis in mammalian cells. *Cell* **109,** 359–369 (2002). doi: 10.1016/S0092-8674(02)00720-1; Medline

38. T. Nguyen, J. Bjorkman, B. C. Paton, D. I. Crane, Failure of microtubule-mediated peroxisome division and trafficking in disorders with reduced peroxisome abundance. *J. Cell Sci.* **119**, 636–645 (2006). doi: 10.1242/jcs.02776; Medline

39. M. Schrader, J. K. Burkhardt, E. Baumgart-Vogt, G. Lüers, H. Spring, A. Völkl, H. D. Fahimi, Interaction of microtubules with peroxisomes. Tubular and spherical peroxisomes in HepG2 cells and their alterations induced by microtubule-active drugs. *Eur. J. Cell Biol.* **69**, 24–35 (1996). Medline

40. D. Hoepfner, M. van den Berg, P. Philippsen, H. F. Tabak, E. H. Hettema, A role for Vps1p, actin, and the Myo2p motor in peroxisome abundance and inheritance in *Saccharomyces cerevisiae*. *J. Cell Biol.* **155**, 979–990 (2001). doi: 10.1083/jcb.200107028; Medline

41. S. Kredel, F. Oswald, K. Nienhaus, K. Deuschle, C. Röcker, M. Wolff, R. Heilker, G. U. Nienhaus, J. Wiedenmann, mRuby, a bright monomeric red fluorescent protein for labeling of subcellular structures. *PLOS ONE* **4**, e4391 (2009). doi: 10.1371/journal.pone.0004391; Medline

42. P. Bharti, W. Schliebs, T. Schievelbusch, A. Neuhaus, C. David, K. Kock, C. Herrmann, H. E. Meyer, S. Wiese, B. Warscheid, C. Theiss, R. Erdmann, PEX14 is required for microtubule-based peroxisome motility in human cells. *J. Cell Sci.* **124**, 1759–1768 (2011). doi: 10.1242/jcs.079368; Medline

43. L. Seldin, A. Muroyama, T. Lechler, NuMA-microtubule interactions are critical for spindle orientation and the morphogenesis of diverse epidermal structures. *eLife* **5**, e12504 (2016). doi: 10.7554/eLife.12504; Medline

44. S. Gallini, M. Carminati, F. De Mattia, L. Pirovano, E. Martini, A. Oldani, I. A. Asteriti, G. Guarguaglini, M. Mapelli, NuMA phosphorylation by Aurora-A orchestrates spindle orientation. *Curr. Biol.* **26**, 458–469 (2016). doi: 10.1016/j.cub.2015.12.051; Medline

45. S. Kotak, C. Busso, P. Gönczy, NuMA interacts with phosphoinositides and links the mitotic spindle with the plasma membrane. *EMBO J.* **33**, 1815–1830 (2014). doi: 10.15252/embj.201488147; Medline

46. Z. Zheng, Q. Wan, G. Meixiong, Q. Du, Cell cycle–regulated membrane binding of NuMA contributes to efficient anaphase chromosome separation. *Mol. Biol. Cell* **25**, 606–619 (2014). doi: 10.1091/mbc.E13-08-0474; Medline

47. W. Qian, S. Choi, G. A. Gibson, S. C. Watkins, C. J. Bakkenist, B. Van Houten, Mitochondrial hyperfusion induced by loss of the fission protein Drp1 causes ATM-dependent G2/M arrest and aneuploidy through DNA replication stress. *J. Cell Sci.* **125**, 5745–5757 (2012). doi: 10.1242/jcs.109769; Medline

48. A. Fagarasanu, F. D. Mast, B. Knoblach, Y. Jin, M. J. Brunner, M. R. Logan, J. N. M. Glover, G. A. Eitzen, J. D. Aitchison, L. S. Weisman, R. A. Rachubinski, Myosin-driven peroxisome partitioning in *S. cerevisiae*. *J. Cell Biol.* **186**, 541–554 (2009). doi: 10.1083/jcb.200904050; Medline

49. J. L. Rohn, J. V. Patel, B. Neumann, J. Bulkescher, N. Mchedlishvili, R. C. McMullan, O. A. Quintero, J. Ellenberg, B. Baum, Myo19 ensures symmetric partitioning of mitochondria and coupling of mitochondrial segregation to cell division. *Curr. Biol.* **24**, 2598–2605 (2014). doi: 10.1016/j.cub.2014.09.045; Medline

50. P. van Bergejik, M. Adrian, C. C. Hoogenraad, L. C. Kapitein, Optogenetic control of organelle transport and positioning. *Nature* **518**, 111–114 (2015). doi: 10.1038/nature14128; Medline

51. E. R. Ballister S. Ayloo, D. M. Chenoweth, M. A. Lampson, E. L. F. Holzbaur, Optogenetic control of organelle transport using a photocaged chemical inducer of dimerization. *Curr. Biol.* **25**, R407–R408 (2015). doi: 10.1016/j.cub.2015.03.056; Medline

52. L. Duan, D. Che, K. Zhang, Q. Ong, S. Guo, B. Cui, Optogenetic control of molecular motors and organelle distributions in cells. *Chem. Biol.* **22**, 671–682 (2015). doi: 10.1016/j.chembiol.2015.04.014; Medline

53. P. Katajisto, J. Döhla, C. L. Chaffer, N. Pentinmikko, N. Marjanovic, S. Iqbal, R. Zoncu, W. Chen, R. A. Weinberg, D. M. Sabatini, Asymmetric apportioning of aged mitochondria between daughter cells is required for stemness. *Science* **348**, 340–343 (2015). doi: 10.1126/science.1260384; Medline

54. C. Trapnell, A. Roberts, L. Goff, G. Pertea, D. Kim, D. R. Kelley, H. Pimentel, S. L. Salzberg, J. L. Rinn, L. Pachter, Differential gene and transcript expression analysis of RNA-seq experiments with TopHat and Cufflinks. *Nat. Protoc.* **7**, 562–578 (2012). doi: 10.1038/nprot.2012.016; Medline

55. A. Subramanian, P. Tamayo, V. K. Mootha, S. Mukherjee, B. L. Ebert, M. A. Gillette, A. Paulovich, S. L. Pomeroy, T. R. Golub, E. S. Lander, J. P. Mesirov, Gene set enrichment analysis: A knowledge-based approach for interpreting genome-wide expression profiles. *Proc. Natl. Acad. Sci. U.S.A.* **102**, 15545–15550 (2005). doi: 10.1073/pnas.0506580102; Medline

56. T. Iwase, A. Tajima, S. Sugimoto, K.-i. Okuda, I. Hironaka, Y. Kamata, K. Takada, Y. Mizunoe, A simple assay for measuring catalase activity: A visual approach. *Sci. Rep.* **3**, 3081 (2013). doi: 10.1038/srep03081; Medline

57. M. J. Hardman, P. Sisi, D. N. Banbury, C. Byrne, Patterned acquisition of skin barrier function during development. *Development* **125**, 1541–1552 (1998). Medline

58. S. Beronja, G. Livshits, S. Williams, E. Fuchs, Rapid functional dissection of genetic networks via tissue-specific transduction and RNAi in mouse embryos. *Nat. Med.* **16,** 821–827 (2010). doi: 10.1038/nm.2167; Medline